J Mater Sci: Mater Med (2009) 20:301–307
DOI 10.1007/s10856-008-3577-0

Preparation and properties of a novel drug delivery system with both magnetic and biomolecular targeting

Yong Yang · Ji-Sen Jiang · Bing Du · Zhi-Feng Gan · Min Qian · Ping Zhang

Received: 17 April 2008 / Accepted: 22 August 2008 / Published online: 13 September 2008

Abstract By loading doxorubicin (DOX) on 5-carboxyl-fluorescein (FAM) labeled AGKGTPSLETTP peptide (A54) coupled starch-coated iron oxide nanoparticles (SIONs), we prepared a novel aqueous drug delivery system with both magnetic and biomolecular targeting, which was specific to human hepatocellular carcinoma cell line BEL-7402. The saturated extent of adsorption reached 2.0 mg DOX/mg A54-SIONs at 28°C, which provided a rather high dose of DOX loading for application. Tests in vitro demonstrated the specificity of DOX-loaded A54-SIONs to BEL-7402 cells. The microscopy images proved that DOX-loaded A54-SIONs were successfully targeted to tumor tissue of nude mice with an external magnetic field in vivo. MTT assay showed higher cytostatic effect of DOX-loaded A54-SIONs to hepatocellular carcinoma cells BEL-7402 than that of DOX-loaded SIONs.

1 Introduction

The effect of drug not only depends on the properties of drug itself, but also on the way it is delivered. Magnetic targeting has raised extensive interests [1, 2] because of its high delivery efficiency, low toxicity and high retention. Drug-loaded magnetic nanoparticles are accumulated in target tissue area by external magnetic field first, then drug releases from the particles in a controllable way. This is the way magnetic targeting system usually works. For example, Zebli et al. [3] demonstrated specific trapping of polymer capsules functionalized with magnetic and luminescent nanoparticles by modeling the bloodstream in the circulatory system. Kohler et al. [4] prepared Fe_3O_4/methotrexate drug delivery system and targeted it to human cervical cancer cells (HeLa). Cinteza et al. [5] carried out photosensitizer drug with Fe_3O_4/polymeric micelles of PE-PEG and demonstrated magnetically directed delivery to tumor cells in vitro.

Biomolecular targeting, another important method of drug delivery, is also developed rapidly in recent years. Some peptides were selected out using phage display peptide libraries for their specific to cancer cells [6–8]. These peptides are called "homing peptides", which are used as vehicles of drugs. It is proved that conjugating drugs with homing peptides can improve the efficiency of drug delivery. Garsky et al. [9] prepared a peptide-doxorubicin conjugate specific to PSA-secreting tumor cells. It was proved to be more effective in inhibiting human prostate cancer cell growth and tumorigenesis through a series of experiments in vitro and in vivo. Achilefu et al. [10] delivered imagine agent in-DTPA for nuclear imaging to NTR-positive tumors with a NT peptide analogue. Toublan et al. [11] prepared serum albumin microspheres modified with peptides containing an integrin-receptor specific sequence on the surface and targeted it to the integrin receptors that are overexpressed in several tumor types.

Akerman et al. [12] targeted i.v.-injected ZnS-capped CdSe quantum dots to specific vascular sites in mice by homing peptides. The results suggested the potential of homing peptides modified nanoparticles in disease diagnosis and therapy. In our previous works, homing peptide

Y. Yang · J.-S. Jiang (✉) · Z.-F. Gan
Department of Physics, Center of Functional Nanomaterials and Devices, East China Normal University, 3663 North Zhongshan Road, Shanghai 200062, People's Republic of China
e-mail: jsjiang@phy.ecnu.edu.cn

B. Du · M. Qian · P. Zhang
School of Life Science, East China Normal University, Shanghai 200062, People's Republic of China

AGKGTPSLETTP (denoted as A54), which is specific to the human hepatocellular carcinoma cell, labeled with green fluorescent protein (GFP) and green fluorescent 5-carboxyl-fluorescein (FAM) was successfully immobilized on the surfaces of bare magnetite nanoparticles [13] and SIONs [14], respectively. Both A54-GFP immobilized bare magnetite nanoparticles and FAM-A54 immobilized SIONs showed magnetic and biomolecular targeting to the human hepatocellular carcinoma cell. In this work, DOX was loaded on A54-SIONs to prepare a novel aqueous drug delivery system with both magnetic and biomolecular targeting. The specificity and toxicity to human hepatocellular carcinoma cell line BEL-7402 were demonstrated. This drug delivery system shows a potential application in cancer therapy.

2 Materials and methods

2.1 Materials

Iron (III) chloride hexahydrate ($FeCl_3{\cdot}6H_2O$, >99%), iron (II) sulfate heptahydrate ($FeSO_4 \cdot 7H_2O$, >99%), sodium hydroxide (NaOH, ≥96%), sodium metaperiodate ($NaIO_4$, ≥99.5%), sodium borohydride ($NaBH_4$, >96%) were purchased from Sinopharm Chemical Reagent Co., Ltd (China). Doxorubicin hydrochloride (≥98%) was purchased from Sigma-Aldrich. All the other chemicals were analytical grade from local suppliers and used without further purification. Roswell Park Memorial Institute (RPMI) 1,640 medium and fetal calf serum (FCS) were purchased from Invitrogen (Carlsbad, CA, USA). AGKGTPSLETTP peptide (A54) was synthesized by HD Biosciences Ltd (Shanghai, China) and labeled with 5-carboxyl fluorescein (FAM) at each peptide's end. The human hepatocellular carcinoma cell line BEL-7402 and normal liver cell line HL-7702 was purchased from the cell bank of Shanghai Institute for Biological Sciences (Shanghai, China).

2.2 Preparation of A54-SIONs

A54-SIONs were prepared as previously reported [14]. Firstly, SIONs were prepared by chemical coprecipitation of iron salt and NaOH in a polymeric starch aqueous solution under N_2 gas. The prepared SIONs were washed, dialyzed to remove excess starch, and redispersed in phosphate buffer solution (PBS, pH = 7.4). The prepared SIONs were composed of iron oxide core and starch chains coating the core and the dispersion of SIONs in PBS (pH = 7.4) possesses excellent stability. The average hydrodynamic diameter of starch-coated iron oxide nanoparticles (SIONs) was 46 nm [14]. By oxidation with sodium periodate ($NaIO_4$), the hydroxyl groups of SIONs were converted to aldehyde groups. After purified by dialysis, polyaldehyde-SIONs were covalently linked to the remanent amine groups of FAM-A54 by Schiffs' reaction to prepare A54-SIONs. The unstable Schiff's bases were reduced to secondary amide bonds by reduction with $NaBH_4$. After removing redundant FAM-A54 and starch with deionized water, the weight ratio of different portion of A54-SIONs, was $m_{\text{magnitite}}$:m_{starch}:$m_{\text{FAM-A54}}$ = 1:1:0.05.

2.3 Preparation of DOX-loaded A54-SIONs and determination of DOX concentration

Serial concentrations of DOX (5–50 μl) were added to A54-SIONs solution (~100 μl) containing 0.5 mg of A54-SIONs in 2 ml sample cells, and then the solutions were diluted to 1 ml with PBS buffer (pH = 7.4). The sample cells were shaken at constant temperatures (301 K, 318 K, 333 K), 300 rpm for 24 h, then centrifuged in an Anke GL-20G-II centrifuge at 10,000 rpm for 30 min to aggregate magnetic nanoparticles. Concentration of DOX in supernatant was determined by absorbance of supernatant at 497 nm (Unico UV-2802S UV–vis spectrophotometer).

The extent of adsorption of DOX on A54-SIONs was calculated according to Eq. 1:

$$q = V(C_0 - C_e)/m \tag{1}$$

where q, V, C_0 and C_e are extent of adsorption of DOX on A54-SIONs, volume of solution, original concentration and equilibrium concentration of DOX solution, respectively, and m is the mass of A54-SIONs.

Drug loading (DL) was calculated according to Eq. 2:

$$DL = q * 100\% \tag{2}$$

Entrapment efficiency (EE) was calculated as Eq. 3:

$$EE = (C_0 - C_E)/C_0 \tag{3}$$

2.4 Fourier-transform infrared spectroscopy (FTIR) analysis

DOX-loaded A54-SIONs were collected by sedimentation with a help of an external magnetic field using a magnetic stirrer. After washed four times with deionized water, DOX-loaded A54-SIONs were dried in vacuum at 60°C for 24 h. Fourier-transform infrared spectra were obtained using a Nicolet Nexus 670 FTIR spectrometer with a resolution of 0.09 cm^{-1}. A small amount mixture of DOX-loaded A54-SIONs and KBr (quality of nanoparticles: KBr was 1:100) was pressed into a disc for analysis. DOX and A54-SIONs were used as controls.

2.5 Kinetics of DOX release from A54-SIONs

DOX-loaded A54-SIONs were collected by an external magnetic field, and redispersed with 40 ml of PBS buffer

(pH = 7.4) in a 100 ml conical flask. The flask was shaken at 37°C, 300 rpm for 144 h. About 50 μl solution was taken out every 2 h, and the absorbance of supernatant at 497 nm was measured with the UV–vis spectrophotometer. The concentration of DOX in supernatant and the ratio of DOX released from A54-SIONs were figured out.

2.6 Cell culture

BEL-7402 and control cell line HL-7702 were cultured in RPMI 1640/10% FCS at 37°C in a humidified atmosphere containing 5% CO_2, and plated into 96-well plate (1×10^4 cells/well) the day before use.

2.7 Specificity in vitro

Binding specificity of DOX-loaded A54-SIONs and DOX-loaded SIONs (without FAM-A54) to BEL-7402 and HL-7702 cells was studied. Two kinds of nanoparticles with a particle concentration of 50 μg/ml were added to the cell culture media separately. The cells were cultured in 24-well plastic dishes for 2 h and examined using an Olympus BX51TF fluorescence microscopy.

2.8 MTT assay

The in vitro toxicity of DOX-loaded A54-SIONs was tested using MTT assay. BEL-7402/HL-7702 cells were seeded at a density of 1×10^4 cells/well in 96-well plates 24 h prior to the experiment. About 10 μl of PBS solution containing DOX-loaded A54-SIONs (1 mg/ml of A54-SIONs, drug loading of 28.7%, entrapment efficiency of 99.6%) was added in the wells. For comparison, 10 μl of PBS solution containing DOX-loaded SIONs (1 mg/ml of SIONs, drug loading of 28.6%, entrapment efficiency of 95.5%) was added in other wells. PBS buffer was used as control sample. Incubated under 37°C and 5% CO_2 concentration for 48 h. About 10 μl of thioazolyl blue solution (MTT, 1 mg/ml) was added and incubated for 4 h. Then all the mediums were removed. Remnants in the wells were dissolved with dimethyl sulfoxide (DMSO). Color intensity was measured using a plate reader (Bio-Tek, Winooski, Vermont, USA). The effect of drug on cell proliferation was calculated as the percentage inhibition in cell growth with respect to the respective controls.

2.9 Animals

The experimental animals were nude mice bearing human hepatocellular carcinoma cell BEL-7402 xenografts. Human hepatocellular carcinoma cell BEL-7402 was implanted at hypoderm of nude mouse armpit. Tumor size was about 1 cm when the nude mouse was 4–6 weeks old, 20–25 g body weight (purchased from Shanghai Animal Center).

2.10 Specificity in vivo

The targeted organ was the tumor at hypoderm of nude mouse armpit bearing human hepatocellular carcinoma cell BEL-7402 xenografts. The nude mice were anaesthetized slightly and tied on a board. PBS solution containing DOX-loaded A54-SIONs (1 mg/ml of A54-SIONs, drug loading of 28.7%, entrapment efficiency of 99.6%) was intravenously injected in tail with the dose of 5 mg DOX-loaded A54-SIONs/kg body weight. A columned permanent magnet with a magnetic field of 0.5 Tesla was put on the surface of tumor for 2 h. Then nude mice were sacrificed by cervical dislocation. Tumor tissue of nude mice was collected, embedded by paraffin and made sections with HE dye. The sections were examined by optical microscopy.

3 Results and discussion

Figure 1 shows the FTIR spectra of A54-SIONs before and after DOX loading. Broad bands at 3,442 cm^{-1} in Fig. 1a–c were due to O–H stretching vibrations. In case of A54-SIONs (Fig. 1a), the bands at 2,922 cm^{-1} and 2,850 cm^{-1} were assigned to aliphatic C–H stretching vibrations of starch [15, 16]. The bands at 1,154 and 1,081 cm^{-1} were attributed to the stretching vibration of C–O in C–O–H groups, and the band at 1,029 cm^{-1} was attributed to the stretching vibration of C–O in C–O–C groups [17]. The characteristic absorption peak of Fe–O bonds for magnetite crystals should be at 572 cm^{-1} [18]. In our samples, it shifted to 586 ± 1 cm^{-1} (Fig. 1a, c) owing to covalent combination of A54 onto magnetite surfaces [13]. No obvious shift was observed after DOX loading in Fig. 1c, indicating that the loading of DOX didn't affect the structure of magnetite nanoparticals. Figure 1b shows the FTIR spectrum of DOX. The bands at 1,724 cm^{-1} were due to C=O stretching vibration. The bands at 2,974 cm^{-1}, 2,936 cm^{-1} and 2,850 cm^{-1} were attributed to C–H stretching vibrations of DOX. The bands during 1,620 cm^{-1}–1,000 cm^{-1} corresponded to the different quinine and ketone groups of the DOX [19]. These characteristic bands of DOX could also be found in the FTIR spectrum of DOX-loaded A54-SIONs (Fig. 1c), indicating the existence of DOX in the sample. C=O stretching bond of pure DOX at 1,724 cm^{-1} (Fig. 1b) shifted to 1,719 cm^{-1} (Fig. 1c) after DOX loading, and the relative absorbance reduced obviously. These could be ascribed to the formation of C=O···HO [20, 21], hydrogen bonding between C=O group of DOX molecule and OH group of starch.

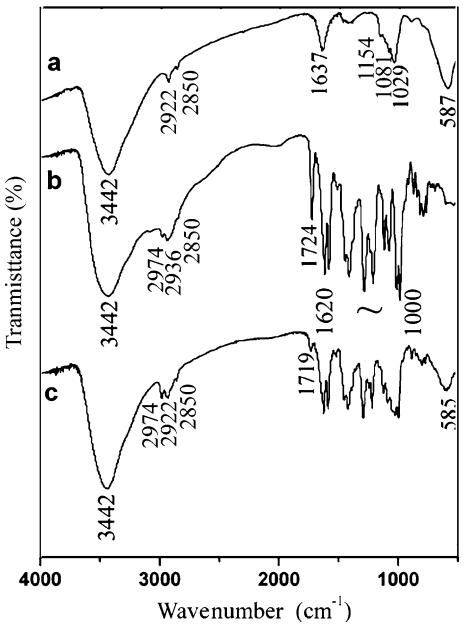

Fig. 1 FTIR spectra of different samples: (a) A54-SIONs; (b) DOX; (c) DOX-loaded A54-SIONs

From FTIR results, we could conclude that DOX-loaded A54-SIONs were obtained by the attachment of C=O group in DOX to the OH group of starch via the formation of hydrogen bonding.

The isotherms characterizing adsorption of DOX onto prepared A54-SIONs are shown in Fig. 2. To compare extent of adsorption at different temperatures, adsorption isotherms at 301 K, 318 K and 333 K were obtained, respectively. The saturated extent of adsorption increased as temperature descended, indicating higher loading ratio of DOX on A54-SIONs at lower temperature. The extent of adsorption increased rapidly as equilibrium concentration rose, and reached its saturation at about 2.0 mg DOX/mg A54-SIONs at 301 K, which was a rather high dose of DOX loading for pharmacological application. According to our previous work [14], a single particle of SIONs (size ~46 nm) is composed of several magnetite crystals (size ~8 nm) enwrapped in starch chains. That is to say, A54-SIONs have a "straw group" structure. Because of the "straw group" structure and plenty of hydroxyl groups of starch, DOX was loaded on A54-SIONs at a rather high dose.

Figure 3 shows release of DOX from DOX-loaded A54-SIONs in PBS solution at pH 7.4, 37°C. The observation of DOX release lasted 150 h. It is found that release rate of DOX was far higher in first 40 h than 40 h later. 68% of DOX was released during 60 h. Hardly any more DOX was released after 60 h. So a sufficient release time could be expected after DOX loaded on A54-SIONs. This result suggested that DOX-loaded A54-SIONs might be a promising drug delivery system because the release of DOX from the surface of A54-SIONs was slow. However, for the biological application of this drug delivery system it is necessary to investigate the DOX release in biological liquids because biological liquids are very different from buffers.

Figure 4 shows the percentage of released DOX in buffer solutions of different pH at 1 h and 37°C. The percentage of released DOX was more than 10% when pH value was lower than 7.0 (pH = 4.0, 6.8). However, the release amount sharply decreased to 3.8% as the pH value rose to neutral (pH = 7.2), and further decreased to around 1% as the pH value rose to basic range (pH = 9.1, 11.0). The pH value of human blood, normal interstitial and tumor interstitial is 7.35–7.45, 7.23, and 6.75 [22–24], respectively. This result shows DOX would probably be released more easily in tumor than in normal tissues from DOX-loaded A54-SIONs in actual pH environment in vivo.

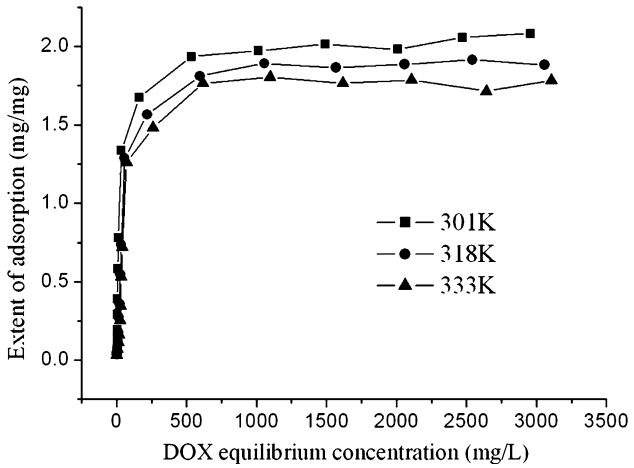

Fig. 2 Adsorption isotherms of DOX on A54-SIONs at different temperatures

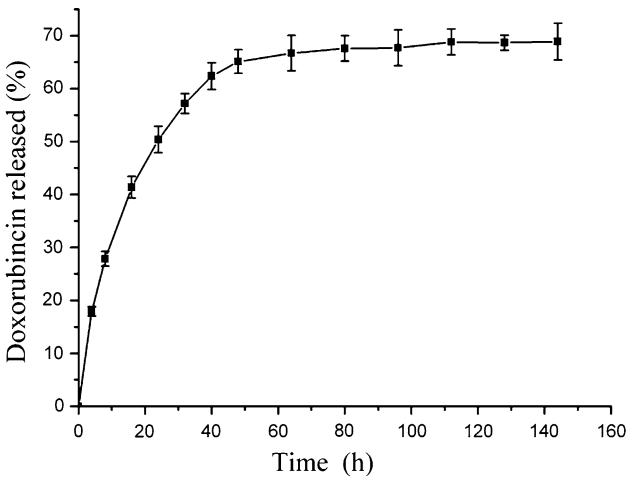

Fig. 3 DOX released from DOX-loaded A54-SIONs at 37°C (pH = 7.4). Error bars were obtained from triplet samples

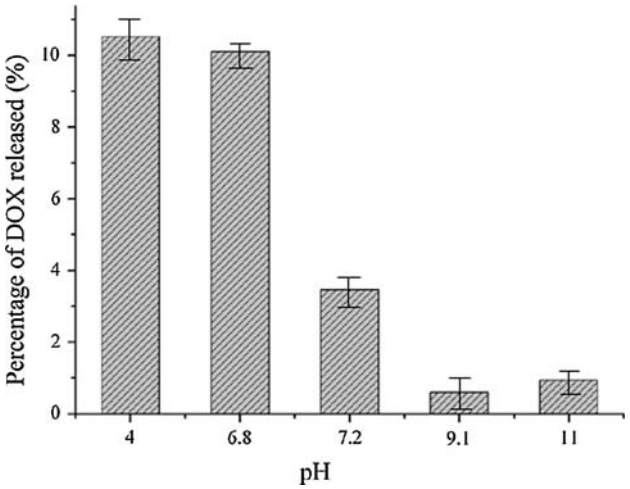

Fig. 4 DOX released from DOX-loaded A54-SIONs at different pH (1 h). Error bars were obtained from triplet samples

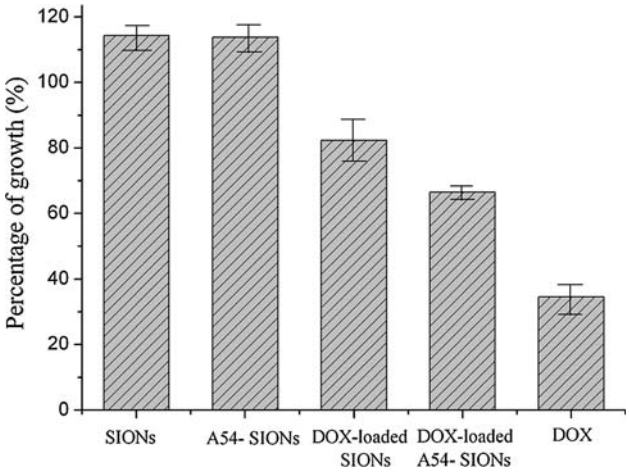

Fig. 6 Cytostatic effect of SIONs and A54-SIONs loaded and unloaded DOX to human hepatocellular carcinoma cell BEL-7402. Error bars were obtained from sextuplet samples

To explore the binding activity and specificity of DOX-loaded A54-SIONs, experiments were conducted in vitro. Figure 5 shows fluorescent images of DOX-loaded A54-SIONs and DOX-loaded SIONs incubated with hepatocellular carcinoma BEL-7402 cells and normal hepatocellular HL-7702 cells. The nuclei in Fig. 5a–d all showed yellow fluorescence which was from the intrinsic fluorescence of DOX. This indicates that a small amount of released DOX from DOX-loaded A54-SIONs and DOX-loaded SIONs entered the nuclei of hepatocellular carcinoma cells and normal hepatocellular cells, because the target of toxic insult of DOX is nuclei [25]. After intensive washing, green fluorescence from fluorescein FAM was observed only on the surface of hepatocellular carcinoma cells (Fig. 5c). This means that DOX-loaded A54-SIONs were decorated on the surface of hepatocellular carcinoma cells. No visible green fluorescence was observed on the normal liver cells (Fig. 5d). This infers that DOX-loaded A54-SIONs did not bind to the normal liver cells. These results show that coupling with homing peptides A54 endowed DOX-loaded SIONs with specific affinity to corresponding tumor cellular in vitro.

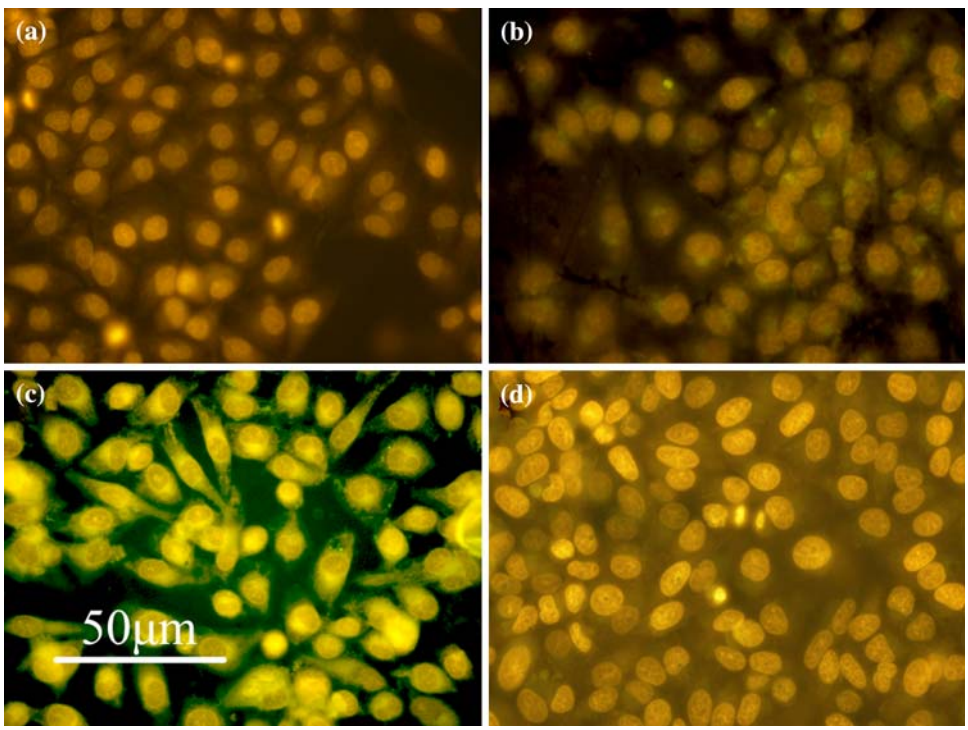

Fig. 5 Fluorescent image of DOX-loaded A54-SIONs and DOX-loaded SIONs incubated with different cell type for 1 h in vitro. (**a**) DOX-loaded SIONs on human hepatocellular carcinoma cell line BEL-7402; (**b**) DOX-loaded SIONs on normal liver HL-7702 cells; (**c**) DOX-loaded A54-SIONs on human hepatocellular carcinoma cell line BEL-7402; (**d**) DOX-loaded A54-SIONs on normal liver HL-7702 cells (×400)

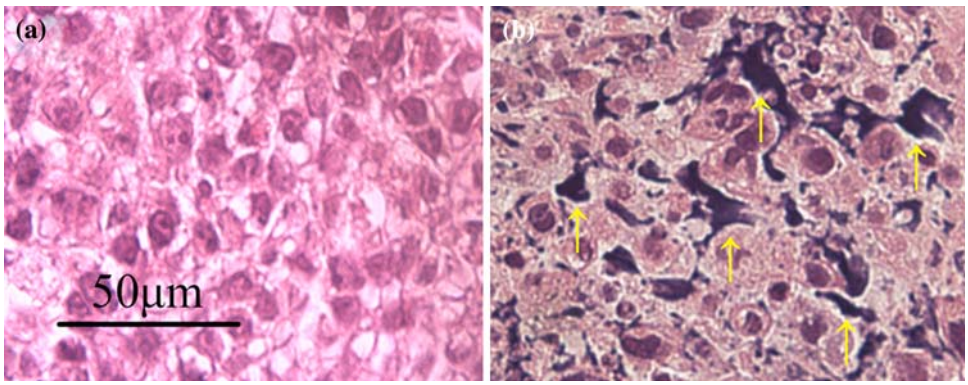

Fig. 7 Tumor tissues of nude mice bearing human hepatocellular carcinoma cell BEL-7402 xenografts. (**a**) control sample without injection; (**b**) intravenously injected with DOX-loaded A54-SIONs solution and attracted with an external magnetic field for 2 h (×1000)

Figure 6 shows the cytotoxicity of different particles against BEL-7402 cells in vitro. The cytotoxic effect was assessed by the percentage of cell growth (PG) [26, 27]. PG was calculated as the ratio of the absorbance of the treated sample to that of the untreated sample determined by the MTT assay. SIONs and A54-SIONs did not cause a cytotoxic effect (PG: 114.3 ± 5.2%, 113.8 ± 4.5%). DOX without carrier showed the highest cytotoxicity (PG: 34.5 ± 6.1%) against BEL-7402 cells. DOX-loaded SIONs (PG: 82.4 ± 3.6%) and DOX-loaded A54-SIONs (PG: 66.5 ± 5.4%) showed lower cytotoxicity against BEL-7402 cells, which might be due to the presence of carriers. Compared with DOX-loaded SIONs, it is obvious that DOX-loaded A54-SIONs showed more cytotoxic to BEL-7402 cells. This result further demonstrates that A54 coupled with SIONs and DOX still possessed specific affinity to hepatocellular carcinoma BEL-7402 cells.

Figure 7 shows tumor tissues of nude mice bearing human hepatocellular carcinoma cell BEL-7402 xenografts before and after intravenously injected with DOX-loaded A54-SIONs solution. Compared with the tumor tissue before intravenously injected with DOX-loaded A54-SIONs solution (Fig. 7a), many black areas (pointed with arrows) were observed in the tumor tissue of nude mice intravenously injected with DOX-loaded A54-SIONs solution and attracted with an external magnetic field for 2 h (Fig. 7b). The black areas could be due to DOX-loaded A54-SIONs accumulating in tumor interstitial. This means that by intravenous injection and external magnetic field, the DOX-loaded A54-SIONs could be targeted to tumor carcinoma cells effectively.

4 Conclusions

Doxorubicin was loaded on A54-SIONs to prepare DOX-loaded A54-SIONs, a novel drug delivery system with both magnetic targeting and biomolecular targeting, which was specific to human hepatocellular carcinoma cell line BEL-7402. The saturated extent of adsorption reached 2.0 mg DOX/mg A54-SIONs at 28°C, which provided a rather high dose of DOX loading for application. DOX was loaded on A54-SIONs with hydrogen bonding. Percentage of released DOX was 68% at 37°C after 60 h in PBS buffer (pH = 7.4). Tests in vitro demonstrated the specificity of DOX-loaded A54-SIONs to BEL-7402 cells. DOX-loaded A54-SIONs were successfully targeted to tumor carcinoma cells by intravenous injection and external magnetic field in nude mice bearing human hepatocellular carcinoma cell BEL-7402 xenografts in vivo. MTT assay showed higher cytostatic effect of DOX-loaded A54-SIONs with both magnetic targeting and biomolecular targeting to hepatocellular carcinoma cells BEL-7402 than DOX-loaded SIONs with simple magnetic targeting.

Acknowledgment This research project is supported by Shanghai Nanotechnology Promotion Center (0652nm009, 0352nm113).

References

1. A.K. Gupta, M. Gupta, Biomaterials **26**, 3995 (2005). doi:10.1016/j.biomaterials.2004.10.012
2. Z.F. Gan, J.S. Jiang, Prog. Chem. **17**, 978 (2005)
3. B. Zebli, A.S. Susha, G.B. Sukhorukov, A.L. Rogach, W.J. Parak, Langmuir **21**, 4262 (2005). doi:10.1021/la0502286
4. N. Kohler, C. Sun, J. Wang, M. Zhang, Langmuir **21**, 8858 (2005). doi:10.1021/la0503451
5. L.O. Cinteza, T.Y. Ohulchanskyy, Y. Sahoo, E.J. Bergey, R.K. Pandey, P.N. Prasad, Mol. Pharm. **3**, 415 (2006). doi:10.1021/mp060015p
6. M. Trepel, W. Arap, R. Pasqualini, Curr. Opin. Chem. Biol. **6**, 399 (2002). doi:10.1016/S1367-5931(02)00336-8
7. O.H. Aina, T.C. Sroka, M.L. Chen, K.S. Lam, Biopolymers **66**, 184 (2002). doi:10.1002/bip.10257
8. R. Pasqualini, E. Ruoslahti, Nature **380**, 364 (1996). doi:10.1038/380364a0
9. V.M. Garsky, P.K. Lumma, D.M. Feng, J. Wai, H.G. Ramjit, M.K. Sardana et al., J. Med. Chem. **44**, 4216 (2001). doi:10.1021/jm0101996
10. S. Achilefu, A. Srinivasan, M.A. Schmidt, H.N. Jimenez, J.E. Bugaj, J.L. Erion, J. Med. Chem. **46**, 3403 (2003). doi:10.1021/jm030081k
11. F.J.-J. Toublan, S. Boppart, K.S. Suslick, J. Am. Chem. Soc. **128**, 3472–3473 (2006). doi:10.1021/ja0544455

12. M.E. Åkerman, W.C.W. Chan, P. Laakkonen, S.N. Bhatia, E. Ruoslahti, Proc. Natl. Acad. Sci. U.S.A. **99**, 12617 (2002). doi:10.1073/pnas.152463399
13. Z.F. Gan, J.S. Jiang, Y. Yang, B. Du, M. Qian, P. Zhang, J. Biomed. Mater. Res. A **84A**, 10 (2008). doi:10.1002/jbm.a.31181
14. J.S. Jiang, Z.F. Gan, Y. Yang, B. Du, M. Qian, P. Zhang, J. Nanopart. Res. (revised)
15. D.K. Kweon, D.S. Cha, H.J. Park, S.T. Lim, J. Appl. Polym. Sci. **78**, 986 (2000). doi:10.1002/1097-4628(20001031)78:5<986::AID-APP70>3.0.CO;2-T
16. J. Zhang, S. Rana, R.S. Srivastava, R.D.K. Misra, Acta Biomater. **4**, 40 (2008). doi:10.1016/j.actbio.2007.06.006
17. R.C. Mundargi, N.B. Shelke, A.P. Rokhade, S.A. Patil, T.M. Aminabhavi, Carbohydr. Polym. **71**, 42 (2008). doi:10.1016/j.carbpol.2007.05.013
18. R.D. Waldron, J. Phys. Rev. **99**, 1727 (1955). doi:10.1103/PhysRev.99.1727
19. S. Rana, A. Gallo, R.S. Srivastava, R.D.K. Misra, Acta Biomater. **3**, 233 (2007). doi:10.1016/j.actbio.2006.10.006
20. G. Smulevich, A. Feis, J. Phys. Chem. **90**, 6388 (1986). doi:10.1021/j100281a064
21. N. Strekal, A. German, G. Gachko, A. Maskevich, S. Maskevich, J. Mol. Struct. **563–564**, 183 (2001). doi:10.1016/S0022-2860(01)00512-9
22. G.R. Martin, R.K. Jain, Cancer Res. **54**, 5670 (1994)
23. I.F. Tannock, D. Rotin, Cancer Res. **49**, 4373 (1989)
24. K. Engin, D.B. Leeper, J.R. Cater, A.J. Thistlethwaite, L. Tupchong, J.D. McFarlane, Int. J. Hyperther. **11**, 211 (1995). doi:10.3109/02656739509022457
25. H. Simpkins, L.F. Pearlman, L.M. Thompson, Cancer Res. **44**, 613 (1984)
26. T.K. Jain, M.A. Morales, S.K. Sahoo, D.L. Leslie-Pelecky, V. Labhasetwar, Mol. Pharm. **2**, 194 (2005). doi:10.1021/mp0500014
27. N. Nasongkla, E. Bey, J. Ren, H. Ai, C. Khemtong, J.S. Guthi et al., Nano. Lett. **6**, 2427 (2006). doi:10.1021/nl061412u